High thermal conductivity of high-quality monolayer boron nitride and its thermal expansion

Thermal conductivity and expansion of high-quality monolayer and few-layer boron nitride

Qiran Cai,[1] Declan Scullion,[2] Aleksey Falin,[1] Kenji Watanabe,[3] Takashi Taniguchi,[3] Ying Chen,[1] Elton J. G. Santos[2] and Lu Hua Li[1]**

1. Institute for Frontier Materials, Deakin University, Geelong Waurn Ponds Campus, Victoria 3216, Australia.

2. School of Mathematics and Physics, Queen's University Belfast, Belfast BT7 1NN, United Kingdom.

3. National Institute for Materials Science, Namiki 1-1, Tsukuba, Ibaraki 305-0044, Japan.

KEYWORDS: thermal conductivity, thermal expansion coefficient, atomically thin boron nitride, 2D materials, Raman spectroscopy.

ABSTRACT: Two-dimensional (2D) materials provide new opportunities for thermal management. Despite of the extraordinarily high thermal conductivity (κ) of graphene, its electrical conduction limits its direct use in thermal management. Atomically thin hexagonal boron nitride (BN) is a wide bandgap 2D material promising for heat dissipation, but κ of monolayer BN and

the potential thickness effect have never been experimentally revealed. Here, we report that high-qualty and clean atomically thin BN has one of the highest thermal conductivity coefficients among electrical insulators, and its κ increases with reduced thickness. Our large-scale molecular dynamic simulations using Green-Kubo formalism accurately reproduce the trend and show the main scattering mechanism. In addition, for the first time we experimentally measured the thermal expansion coefficients (TECs) of 1-3L BN at 300-400 K, which are compared with atomistic *ab initio* density functional theory (DFT) calculations in a wider range of temperatures. Our results indicate that atomically thin BN is a favorable candidate for heat dissipation applications.

With the increasing demand in miniaturization, thermal dissipation becomes critical for the performance, reliability, longevity, and safety of various products, such as electronic and optoelectronic devices, lithium ion batteries, and micro-machines. Two-dimensional (2D) materials, such as graphene, show outstanding thermal transport. At near room-temperature, the in-plane thermal conductivity (κ) of mechanically exfoliated and high-quality chemical vapor deposition- (CVD-) grown suspended graphene was measured to be mostly in the range of 1800-5300 W/mK[1-3] and 1200-3100 W/mK,[4-10] respectively. Intriguingly, thickness plays an important role in κ of few-layer graphene. Balandin et al. found that κ of graphene dropped from ~4000 to ~2700 and ~1300 W/mK from 1 to 2 and 4 layers, respectively.[11] It should be noted that defects, grain boundaries, folding/wrinkles, and surface contaminations (*e.g.* polymer residues from transfer process) greatly deteriorate κ of graphene due to the scattering of low frequency phonons.[6,9,12] However, the electrical conductivity of graphene prevents it from being directly used in many thermal dissipation applications, such as in electronics. It is highly desirable to explore electrically insulating materials with excellent thermal conductivity.

Boron nitride (BN) nanosheets, atomically thin hexagonal boron nitride (hBN), have an analogous structure to that of graphene, and are one of the strongest electrically insulating materials.[13] Atomically thin BN nanosheets have a wide bandgap of ~6 eV, which is not sensitive to thickness change.[14] BN is an excellent dielectric substrate for graphene, molybdenum disulfide (MoS_2), and many other 2D material-based electronic and optical devices.[15,16] In addition, BN nanosheets are much more resistant to oxidation at elevated temperatures.[17] The electrical insulation and high thermal stability make BN nanosheets better than graphene in the oxidation and corrosion protection of metal surfaces as well as air-sensitive 2D materials without galvanic corrosion.[18-22] The use of atomically thin BN in this aspect has been further extended to the coverage of plasmonic metal nanoparticles for surface enhanced Raman spectroscopy, enabling much improved sensitivity, reproducibility, and reusability.[23,24] Enhanced surface adsorption capabilities have also been observed in atomically thin BN.[25]

HBN has long been under the radar in the search of heat dissipating materials. The in-plane thermal conductivity of highly oriented pyrolytic hBN (HOPBN) was measured to be up to ~400 W/mK at room temperature, but it should be emphasized that the HOPBN used in this early study consisted of small crystallites (hence grain boundaries) and contained defects and dislocations.[26,27] More recently, there have been a large number of attempts to utilize 2D BN as fillers in composites or thermal interface materials for thermal management.[28-37] It has also been found that BN substrate can cool 2D transistors on its top by its emission of hyperbolic phonon polariton.[38] Despite of some theoretical studies,[39-44] the thermal conductivity of monolayer BN as well as the comprehensive investigation on the thickness effect on κ of atomically thin BN have never been experimentally investigated. Jo et al. reported the first experimentally-derived κ of few-layer BN. The κ of 5 and 11 layer (L) thick BN were ~250 and ~360 W/mK at room temperature,

respectively.[45] The worse heat spreading property of the 5L BN was explained by polymer residues from sample preparation process. One year later, Zhou et al. used Raman spectroscopy to find κ of CVD-grown 9L BN in the range of 227-280 W/mK.[46] Although suspended CVD-grown 1L and 2L BN sheets were also prepared, no Raman signals could be detected presumably due to sample quality or contamination issues, and hence κ of 1-2L BN was not assessable in this study. Alam et al. and Lin et al. also studied κ of ~30-60L and few-layer CVD-grown BN.[47,48] Note that poly(methyl methacrylate)- (PMMA-) assisted transfer was used in all these four abovementioned studies, and, as reported previously, the process inevitably leaves polymer residues which causes phonon scattering.[49] More recently, Wang et al. used polydimethylsiloxane (PDMS) to transfer a 2L BN exfoliated from commercial hBN powder onto pre-patterned thermometers and observed a thermal conductivity of 484+141/−24 W/mK at room temperature.[50] According to our experience and previous reports, PDMS also leaves a certain amount of contamination that is more difficult to eliminate than PMMA.[51] On the other hand, the thermal expansion coefficients (TECs) of atomically thin BN has not been experimentally studied either, though contradictory theoretical values have been reported.

Here, we report for the first time the thermal conductivity coefficients, thermal expansion coefficients, and their thickness-dependence of clean and high-quality 1-3L BN, which were directly mechanically exfoliated from hBN single crystals onto gold (Au) coated micro-wells without polymer-based transfer process. The optothermal Raman technique-deduced κ of the atomically thin BN increased with reduced thickness: 733±157, 605±132, 526±97 W/mK for 1-3L BN at close-to room temperature, respectively, despite that we found that the visible light absorption of atomically thin BN was much smaller than those estimated previously. The TECs of 1-3L BN were also experimentally revealed for the first time. The excellent thermal conductivity,

electrical insulation, atomic thickness, high strength, superb thermal and chemical stability make atomically thin BN an attractive material in various heat dissipation applications.

The atomically thin BN samples were mechanically exfoliated from high-quality hBN single crystals[52,53] using Scotch tape onto Au coated Si wafer with pre-fabricated micro-wells (diameter: 3.8 μm) and connecting trenches (width: 0.2 μm). The trenches acted as vents to avoid the trapped air in BN-covered micro-wells from expansion during heating. According to our previous studies, the atomically thin BN sheets prepared by this method were almost free of defects and grain boundaries.[13,17] The absence of polymer-based transfer process prevented surface contaminations that could deteriorate thermal conductivity. Optical microscope was used to locate atomically thin sheets, followed by atomic force microscopy (AFM) measurements to determine their thickness. Figure 1 shows the optical and AFM images of a 1L BN suspended over four micro-wells. According to AFM height trace (Figure 1c), it had a thickness of 0.52 nm, typical for 1L BN.[16,17,54] Figure 1d compares the Raman spectra of suspended 1-3L and bulk BN, whose *G* band frequencies were 1367.5, 1366.8, 1366.8, and 1366.3 cm^{-1}, respectively. As shown in our previous study, the phonon frequencies of E_{2g} vibrations in suspended atomically thin BN were close to that of bulk hBN due to the absence of substrate-induced strain.[54]

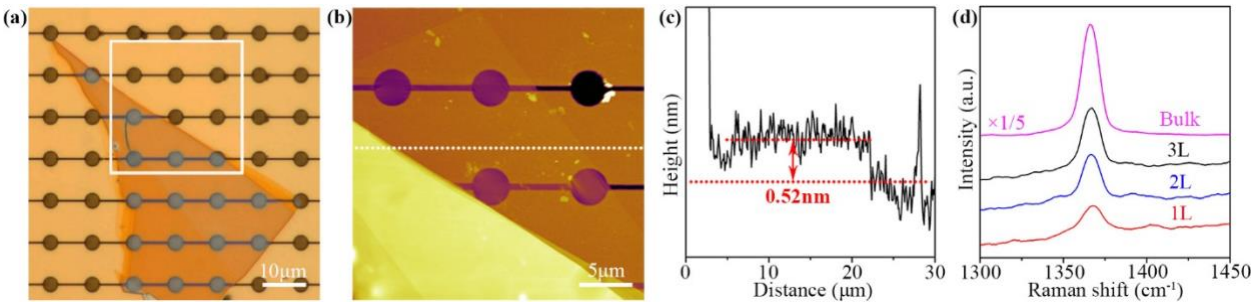

Figure 1. (a) Optical microscopy photo of a 1L BN suspended over 4 micro-wells in Au coated Si substrate; (b) the AFM image corresponding to the square in (a); (c) the height trace from the AFM scans; (d) Raman spectra of the suspended 1-3L and bulk BN.

We used optothermal Raman technique to measure κ of the high-quality atomically thin BN.[1,3-5,46,55,56] First, the temperature-dependent Raman spectra of the suspended 1-3L and bulk BN were recorded to determine their temperature coefficients. In these measurements, relatively small laser powers of 0.84−1.63 mW were used to minimize the effect of laser heating. Figure 2a displays the typical Raman spectra of the suspended 1L BN in the range of 343-423 K (see Supporting Information Figure S2 for 2-3L BN). All samples showed downshifted Raman *G* bands with increased temperature. Linear fittings, *i.e.* $\omega - \omega_0 = \chi T$, were applied to estimate the first-order temperature coefficient (χ), where $\omega - \omega_0$ is the change of the *G* band frequency due to temperature variation, and T is temperature. χ for the suspended 1-3L BN, *i.e.* −0.0187±0.0019, −0.0196±0.0013, and −0.0199±0.0006 cm^{-1}/K, respectively (Figure 2b-d), were quite close to that of suspended bulk hBN single crystals, which was −0.0191±0.0005 cm^{-1}/K (see Supporting Information Figure S3). In addition, these values were in good agreement with two reports on other BN nanomaterials.[37,57] The observed Raman downshifts with increased temperature was mainly caused by strong anharmonic phonon-phonon effects, softening the vibrational mode.[57,58]

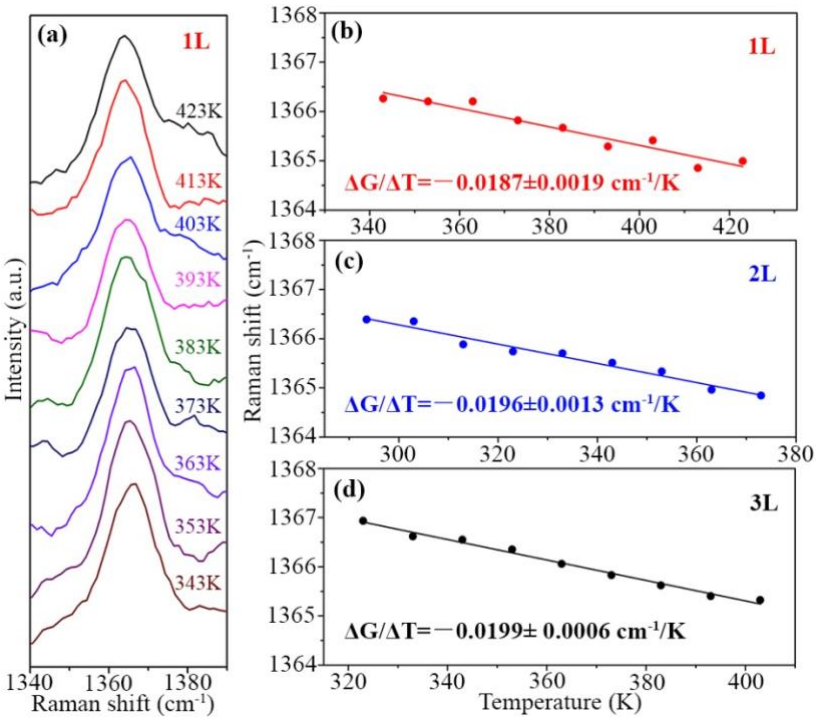

Figure 2. (a) Raman *G* bands of the suspended 1L BN at stage temperatures between 343 and 423 K; (b-d) the corresponding *G* band frequencies as a function of temperature and linear fittings of 1-3L BN.

Next, the effect of laser heating on the Raman frequency of the suspended 1-3L BN was investigated. The total laser power absorbed by the BN (Q) equals to the multiplication of the absorbance (I_{ab}) of BN with the laser power (P). It was reported that absorbance could greatly affect the Raman-deduced thermal conductivity of graphene.[3,4] For the measurements of the light absorbance, we transferred atomically thin BN exfoliated from hBN single crystals on SiO_2/Si substrate to a transparent quartz plate by PMMA, and the polymer was removed by heating in air. The absorbance of BN was estimated by the deduction of the light absorption of the quartz without consideration of the weak light reflection of 2D sheets.[59,60] The absorbance values for 1-4L BN were 0.43±0.11%, 0.66±0.10%, 1.00±0.07%, and 1.09±0.02%, respectively (see Supporting

Information Figure S4). These values were much smaller than those used in previous studies. Zhou et al. measured the absorbance of 1-2L and 9L CVD-grown BN transferred to glass slides, and the values were 1.5% and 5.1% at 514.5 nm wavelength, respectively.[46] Lin et al. obtained an absorbance of ~3% for a 2.1 nm-thick (6L) CVD-grown BN transferred to a quartz substrate.[48] For cross-checking purpose, we can roughly extrapolate the absorbance based on the UV/Vis spectra of CVD-grown 1L BN reported elsewhere,[61,62] and the absorbance was <1%. The very small absorbance is reasonable if one considers the wide bandgap (*i.e.* ~6 eV) of high-quality or defect-free atomically thin BN, which should have minimal light absorption at 514.5 nm (*i.e.* ~2.4 eV).

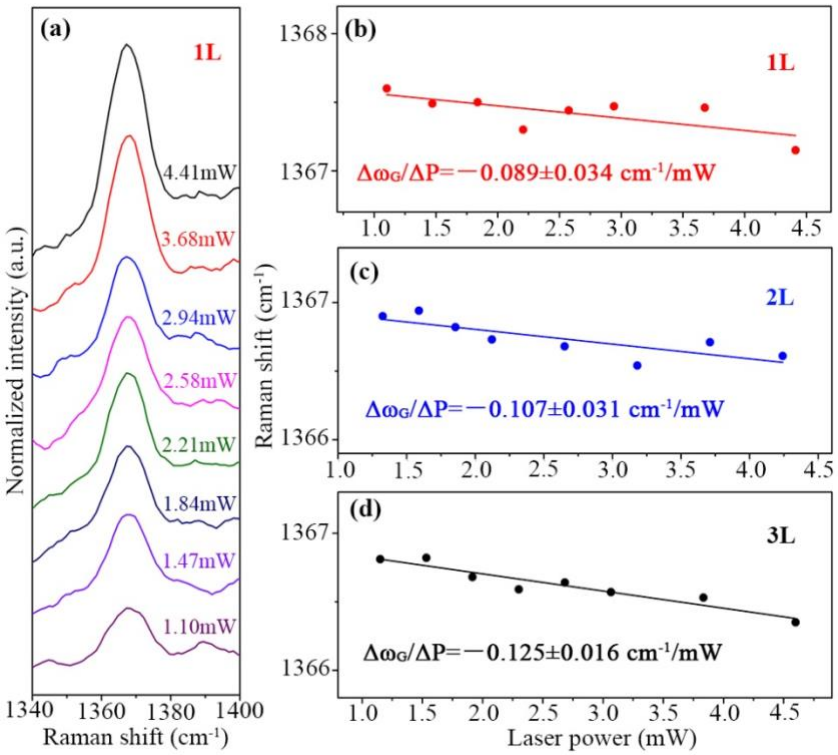

Figure 3. (a) Raman *G* bands of the suspended 1L BN under laser power of 1.10-4.41 mW; (b-d) the corresponding *G* band frequencies as a function of laser power and linear fittings of 1-3L BN.

Figure 3(a) exemplifies the Raman spectra of the *G* bands of the suspended 1L BN under different laser power (see Supporting Information Figure S5 for 2-3L BN). The Raman downshifts were observed in all samples, suggesting increased local temperature with incremental laser power. However, such temperature increase was far from dramatic (*i.e.* ~25 K) partially due to atomically thin BN's small absorption of 514.5 nm light. We linearly fitted the *G* band frequencies as a function of the laser power, and the derived slopes for the suspended 1-3L BN were −0.089±0.034, −0.107±0.031, and −0.125±0.016 cm^{-1}/mW, respectively (Figure 3b-d).

The laser-induced Raman frequency change of the suspended atomically thin BN sheets correlated to their capabilities of thermal conduction to the edge of the micro-wells where the Au film served as a heat sink kept at ambient temperature. If heat loss via air and radiation is ignored, the temperature distribution $T(r)$ in the suspended BN can be written as:[4]

$$T(r) = T_1 + \frac{Q}{2\pi d\kappa}\ln\left(\frac{R}{r}\right)\beta(r), \quad r \le R \qquad (1)$$

where T_1 is the temperature at the edge of the suspended BN (*i.e.* the boundary condition, $T(R) = T_1$); Q is the absorbed laser power; d is BN thickness; κ is thermal conductivity; R is the radius of the micro-well (1.9 μm).

$$\beta(r) = 1 + \frac{Ei\left(-\frac{r^2}{r_0^2}\right) - Ei\left(-\frac{R^2}{r_0^2}\right)}{2\ln\left(\frac{R}{r}\right)} \qquad (2)$$

where r_0 is the radius of the laser beam, which was estimated to be 0.31±0.01 μm by performing a Raman line scan of the edge of a 80 nm gold covered Si wafer (see Supporting Information Figure S6).[4] Note that r_0 was much smaller than the radius of the micro-wells. The Raman-measured temperature (T_m) of the suspended BN can be estimated by:

$$T_m \approx \frac{\int_0^R T(r)\exp(-\frac{r^2}{r_0^2})r\,dr}{\int_0^R \exp(-\frac{r^2}{r_0^2})r\,dr} \quad (3)$$

Given that the thermal resistance between the atomically thin BN and Au heat sink was negligible due to the relatively large contact area, the thermal conductivity of the suspended BN can be approximated as:

$$\kappa = \frac{\ln(\frac{R}{r_0})}{2\pi d\frac{T_m - T_a}{Q}}\alpha \quad (4)$$

where α is the Gaussian profile factor of the laser beam:

$$\alpha = \frac{T_m - T_1}{T_0 - T_1}\beta(r_0) \quad (5)$$

where T_0 is the temperature of the suspended BN at radial distance of r_0. In our experimental setup, $\frac{T_m - T_1}{T_0 - T_1}$ is ~1.03 and $\beta(r_0)$ is ~0.94, so α is 0.97. T_a is the ambient temperature; $\frac{T_m - T_a}{Q}$ denotes the increased temperature of the center of the suspended BN due to the absorbed laser power and can be deduced from the slopes in Figure 2 and 3. The thermal conductivities of the suspended 1-3L BN were calculated to be 733±157, 605±132, 526±97 W/mK, respectively (Figure 4a, red circle). Note we also used the same procedure to measure κ of monolayer graphene, which gave a value of 2070±110 W/mK (see Supporting Information S7).

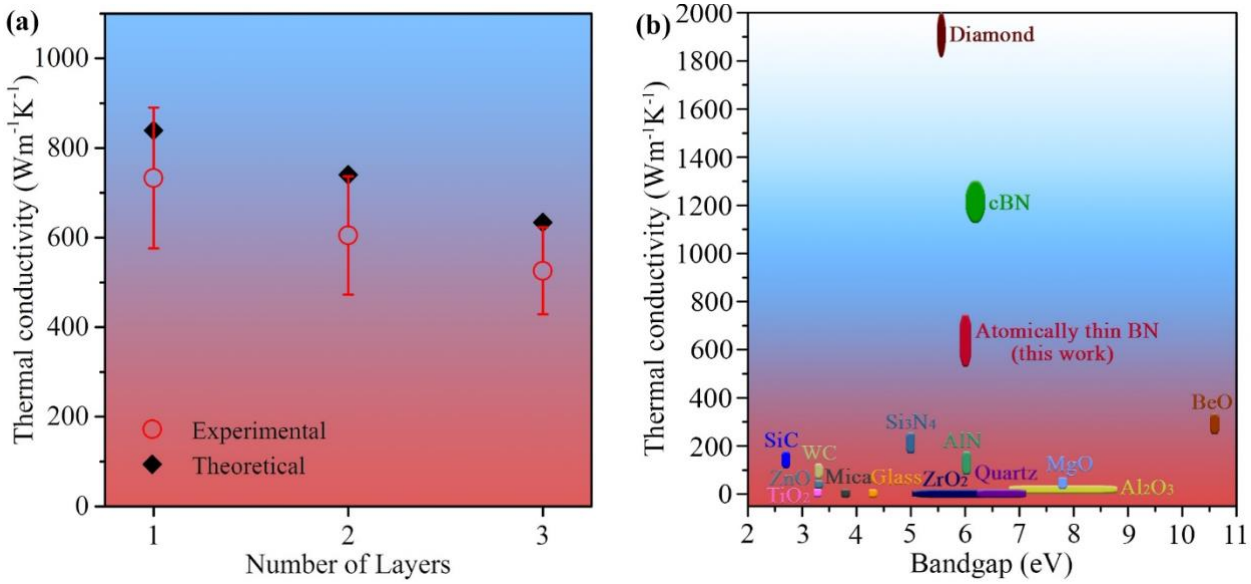

Figure 4. (a) Experimental (red) and theoretical (black) thermal conductivity coefficients of high-quality 1-3L BN; (b) comparison of the thermal conductivity of some common semi-conductors and insulators.

Molecular dynamics (MD) calculations (see Methods for details) were conducted on the thermal conductivity of atomically thin BN. The theoretical coefficients of 849, 740, and 634 W/mK for 1-3L BN at room temperature, respectively are in agreement with the experimental ones (Figure 4a, black rhombus). Our calculated value of 1L BN is close to ~800 W/mK reported by Lindsay *et al.* by considering a 10 μm grain size.[40] The experimental trend that κ of BN increased with reduced thickness was also observed in our simulations. Graphene also shows such a phenomenon, which was explained by the cross-plane coupling of the low-energy phonons and increased Umklapp scattering in few-layer graphene.[11,63] Such mechanism is also applicable to atomically thin BN.[40] Any additional layers added to 1L BN creates more ZA, TA and LA phonon states available for Umklapp scattering, which is the dominating limitation in the thermal conductivity of single-

crystalline and defect-free atomically thin BN at room temperature (see Supporting Information, Figure S8).

The thermal conductivities of some common semi-conductors and insulators as a function of their bandgaps are compared in Figure 4b. Diamond, cubic boron nitride (cBN), and atomically thin BN are the best thermal conductors with bandgaps larger than 5.5 eV. Nevertheless, atomically thin BN has the lowest density (<2.0 g/cm^3) in comparison to those of diamond (3.51 g/cm^3) and cBN (3.45 g/cm^3).

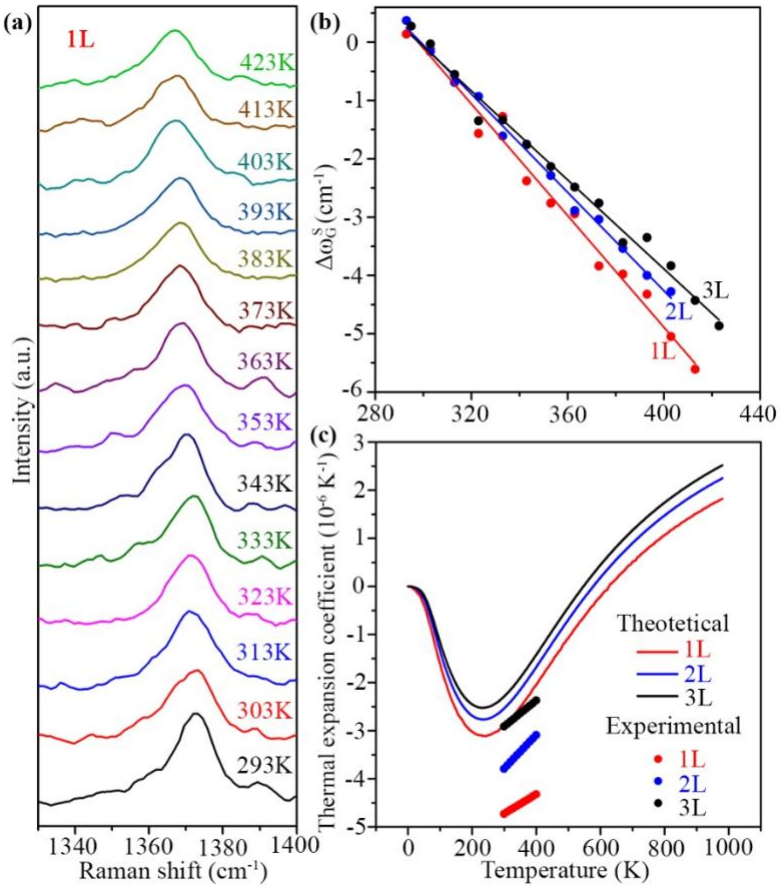

Figure 5. (a) Raman *G* bands of the SiO_2 substrate supported 1L BN at diffrent temperatures between 293K and 423 K; (b) the corresponding *G* band frequency shift as a function of

temperature and linear fittings of 1-3L BN using TEC as fitting parameter. (c) Experimental (dots) and theoretical (lines) curves of the thermal expansion coefficients of 1-3L BN.

In addition, we also used the optothermal Raman technique to estimate TECs of atomically thin BN of different thicknesses. The frequency shifts of the Raman *G* band of substrate-bound 1-3L BN in the temperature range of 293-423 K were recorded (Figure 5a, b and Figure S9). The frequency downshifts with increased temperature could be caused by three factors: 1) the thermal expansion of BN lattice ($\Delta\omega_G^E$); 2) anharmonic effects ($\Delta\omega_G^A$); 3) the TEC mismatch between the atomically thin BN and the SiO_2/Si substrate. As atomically thin BN sheets are insulators, doping effect due to substrate was negligible.[25,64] Therefore, the temperature-dependent *G* band shift ($\Delta\omega_G$) of substrate-bound BN nanosheets could be written as:

$$\Delta\omega_G = \Delta\omega_G^E(T_m) + \Delta\omega_G^A(T_m) + \Delta\omega_G^S(T_m) \quad (6)$$

where T_m is the measured temperature of the sample; $\Delta\omega_G^S(T_m)$ is the effect of the strain $\varepsilon(T_m)$ due to the TEC mismatch, which can be expressed as:

$$\Delta\omega_G^S(T_m) = \beta\varepsilon(T_m) = \beta\int_{297}^{T_m}(\alpha_{SiO_2}(T) - \alpha_{BN}(T))dT \quad (7)$$

where β is the biaxial strain coefficient of the *G* band of atomically thin BN. $\beta = 2\gamma\omega_o$, and γ is the Gruneisen parameters of 1-3L BN, which were obtained from our density functional theory (DFT) calculations (see Supporting Information, Figure S10), and ω_o is the strain-free *G* band frequency.[65] Therefore, β values for 1-3L BN are −56.07, −56.03, and −55.99 cm^{-1}/% for 1-3L BN, respectively.[54] α_{SiO_2} and α_{BN} are the temperature-dependent TECs of SiO_2 and BN nanosheets,

respectively. Because our measured temperature-dependent *G* band shifts of the suspended BN nanosheets contribute to only the first two factors mentioned above, we can use the TECs of BN nanosheets as variants to fit the experimental data of the *G* band shifts of the substrate-bound BN nanosheets (Eq. 7) (Figure 5b). The TECs of 1-3L BN were estimated to be $(–4.73±0.01)×10^{-6}$, $(−3.79±0.01)×10^{-6}$ and $(−2.91±0.01)×10^{-6}$/K at room temperature, which are close to the value of hBN.[66] DFT calculations on TECs of 1-3L BN were also performed, and the theoretical and experimental curves are compared in Figure 5c. The difference between the two was due to the limitation of the exchange-correlation functional in representing the fundamental vibrational modes, as recently pointed out.[54]

In summary, suspended high-quality monolayer and few-layer BN sheets were prepared by direct mechanical exfoliation of hBN single crystals without polymer contamination to reveal their intrinsic κ. The Raman-deduced κ for 1-3L BN were 733±157, 605±132, and 526±97 W/mK, respectively. The trend which was reproduced in our MD simulations was caused by the interlayer interaction that results in more phonon branches and states available for Umklapp scattering in few-layer BN. We also experimentally and theoretically investigated the TECs of atomically thin BN, and the experimentally-deduced values were $(–4.73±0.01)×10^{-6}$, $(−3.79±0.01)×10^{-6}$ and $(−2.91±0.01)×10^{-6}$/K for 1-3L BN at room temperature, respectively. This study contributes to the knowledge system on the thermal conductivity of 2D materials and shows that atomically thin BN sheets have much better thermal conductivity than the bulk counterpart and hence are more advantageous in heat dissipation applications.

Methods

Sample preparation and Raman measurement. The trench-connected micro-wells in Si wafer were fabricated by the combination of photolithography and electron beam lithography. The depth for both the micro-wells and trenches was 2 μm. Sputter was used to coat the Au film whose thickness was *in situ* monitored by a quartz balance (EM ACE600, Leica). The suspended atomically thin BN sheets were mechanically exfoliated on the Au coated Si wafer from high-quality hBN single crystals. The optical microscope and AFM were Olympus BX51 and Asylum Research Cypher. A Renishaw inVia micro-Raman system equipped with a 514.5 nm laser was used. In all experiments, a 100× objective lens with a numerical aperture of 0.90 was used. All Raman spectra were calibrated with the Raman band of Si at 520.5 cm^{-1}. The laser power passing the objective lens was measured by an optical power meter (1916-C, Newport). A heating stage (LTS350, Linkam) was used for temperature control. For optical absorbance measurements, atomically thin BN was first exfoliated on SiO_2 (90 nm)/Si substrate and transferred onto quartz with the help of PMMA. To remove the polymer, the samples were heated at 550 °C in air for 3 h.

Molecular dynamics using classical potentials. Thermal conductivity coefficients κ were calculated using the Green-Kubo approach, which was simulated by the integration of the time-dependent heat-flux autocorrelation functions via:

$$k_{ab} = \frac{1}{k_B T^2 V} \int_0^{\infty} \langle J_a(t) J_b(0) \rangle dt$$

where t is the time, T and V are the system temperature and volume, respectively, $J_{\alpha,\beta}$ are the components of the lattice heat current vector $\vec{J}$ along the α and β components. $\langle J_\alpha(t)J_\beta(0)\rangle$ is the ensemble averaged heat current autocorrelation function. In this work $\alpha = \beta$ because the symmetry to the hBN lattice along the in-plane. The heat current vector is defined as

$$\vec{J}(t) = \frac{d}{dt}\sum_i \vec{R}_i E_i = \sum_i E_i \vec{v}_i + \sum_i \frac{dE_i}{dt}\vec{R}_i$$

where $\vec{R_i}$, v_i, and E_i are the position, velocity, and the energy of atom i. Calculations were carried out within MD simulations using LAMMPS.[67] The three-body Tersoff potential[68] was used to treat in-plane interactions and a Lennard-Jones potential[69] was used to treat out-of-plane interactions. The parameters of these potentials have been described elsewhere.[40] The DFT relaxed structures were used as an initial guess and then further minimized within LAMMPS. The system was then equilibrated under an NVT ensemble for 2.5 ns at 300 K. Following this, the Green-Kubo method was used to calculate the thermal conductivity. Calculations were run under an NVE ensemble for 10 ns with a time step of 0.5 fs. The simulated κ values converged within ~5.5 ns, after which the κ magnitudes were averaged and used to determine the final κ reported in this work. Different correlation lengths p of 400, 500 and 600 with a sampling interval s of 10 ps were used along with an effective volume of N_x*2.50*N_y*4.33*N_L*3.33 and 36,000 atoms in the calculation of the thermal conductivity. N_x and N_y are the number of unit cells in the x and y directions respectively, and N_L is the number of layers. To initialize the velocities, LAMMPS used a pseudo random number generator and assigned a velocity to each atom based on a Gaussian distribution. For each calculation (12 in total, 4 for each layer), a different number was use as the seed for the random number generator.

Ab initio density functional theory. Theoretical calculations were carried out within DFT using the Vienna Ab-Initio Simulation package (VASP).[70] The generalized gradient approximation[71] along with many-body dispersion force-corrections[72,73] were utilized along with a well-converged 800 eV plane-wave cut-off. The projector augmented wave (PAW)[74,75] pseudopotentials were utilized to model the bonding environments of B and N. The atomic positions and lattice vectors were allowed to relax until the forces on the atoms and pressure on the cell were less than 0.000005 eV/Å and 0.01 GPa respectively. A 24×24×1 Γ-centered k-grid was used to sample the Brillouin zone. Thermal expansion coefficients were calculated using the Phonopy code,[76] and the quasi-harmonic approximation. A 2×2×1 supercell was used in all phonon calculations. Experimental Details. 12 point, double-spaced. References are superscripted and appear after the punctuation.[6]

ASSOCIATED CONTENT

Supporting Information. The Supporting Information is available free of charge on the ACS Publications website at DOI:XXXX.

AUTHOR INFORMATION

Corresponding Author

* Email: e.santos@qub.ac.uk,

* Email: luhua.li@deakin.edu.au

Author Contributions

The manuscript was written through contributions of all authors. All authors have given approval to the final version of the manuscript. L.H.Li conceived and directed the project. Q.Cai and L.H.Li

prepared the samples and conducted the experiments, and A.Falin did AFM. E.J.G.Santos and D.Scullion did theoretical calculations. K.Watanabe and T.Taniguchi provided hBN single crystals. Y.Chen discussed the results. L.H.Li, Q.Cai and E.J.G.Santos co-wrote the manuscript with input from all authors.

Notes

The authors declare no completing financial interest.

ACKNOWLEDGMENT

L.H.Li thanks the financial support from Australian Research Council (ARC) via Discovery Early Career Researcher Award (DE160100796). Q.Cai acknowledges ADPRF from Deakin University. Part of the work was done at the Melbourne Centre for Nanofabrication (MCN) in the Victorian Node of the Australian National Fabrication Facility (ANFF). D.Scullion thanks his EPSRC studentship. E.J.G.Santos acknowledges the use of computational resources from the UK national high performance computing service (ARCHER) for which access was obtained via the UKCP consortium (EPSRC grant ref EP/P022626/1); the UK Materials and Molecular Modelling Hub for access to THOMAS supercluster, which is partially funded by EPSRC (EP/P020194/1). The Queen's Fellow Award through the grant number M8407MPH, the Enabling Fund (A5047TSL), and the Department for the Economy (USI 097) are also acknowledged.

REFERENCES

(1) Balandin, A. A.; Ghosh, S.; Bao, W. Z.; Calizo, I.; Teweldebrhan, D.; Miao, F.; Lau, C. N. *Nano Lett.* **2008,** *8*, 902-907.
(2) Ghosh, S.; Calizo, I.; Teweldebrhan, D.; Pokatilov, E. P.; Nika, D. L.; Balandin, A. A.; Bao, W.; Miao, F.; Lau, C. N. *Appl. Phys. Lett.* **2008,** *92*, 151911.
(3) Lee, J. U.; Yoon, D.; Kim, H.; Lee, S. W.; Cheong, H. *Phys. Rev. B* **2011,** *83*, 081419.

(4) Cai, W. W.; Moore, A. L.; Zhu, Y. W.; Li, X. S.; Chen, S. S.; Shi, L.; Ruoff, R. S. *Nano Lett.* **2010,** *10*, 1645-1651.
(5) Chen, S. S.; Moore, A. L.; Cai, W. W.; Suk, J. W.; An, J. H.; Mishra, C.; Amos, C.; Magnuson, C. W.; Kang, J. Y.; Shi, L.; Ruoff, R. S. *ACS Nano* **2011,** *5*, 321-328.
(6) Chen, S. S.; Li, Q. Y.; Zhang, Q. M.; Qu, Y.; Ji, H. X.; Ruoff, R. S.; Cai, W. W. *Nanotechnol.* **2012,** *23*, 365701.
(7) Jauregui, L. A.; Yue, Y.; Sidorov, A. N.; Hu, J.; Yu, Q.; Lopez, G.; Jalilian, R.; Benjamin, D. K.; Delkd, D. A.; Wu, W.; Liu, Z.; Wang, X.; Jiang, Z.; Ruan, X.; Bao, J.; Pei, S. S.; Chen, Y. P. *ECS Transactions* **2010,** *28*, 73-83.
(8) Xu, X. F.; Pereira, L. F. C.; Wang, Y.; Wu, J.; Zhang, K. W.; Zhao, X. M.; Bae, S.; Bui, C. T.; Xie, R. G.; Thong, J. T. L.; Hong, B. H.; Loh, K. P.; Donadio, D.; Li, B. W.; Ozyilmaz, B. *Nat. Commun.* **2014,** *5*, 3689.
(9) Malekpour, H.; Ramnani, P.; Srinivasan, S.; Balasubramanian, G.; Nika, D. L.; Mulchandani, A.; Lake, R. K.; Balandin, A. A. *Nanoscale* **2016,** *8*, 14608-14616.
(10) Li, H. Y.; Ying, H.; Chen, X. P.; Nika, D. L.; Cocemasov, A. I.; Cai, W. W.; Balandin, A. A.; Chen, S. S. *Nanoscale* **2014,** *6*, 13402-13408.
(11) Ghosh, S.; Bao, W. Z.; Nika, D. L.; Subrina, S.; Pokatilov, E. P.; Lau, C. N.; Balandin, A. A. *Nat. Mater.* **2010,** *9*, 555-558.
(12) Yang, N.; Ni, X. X.; Jiang, J. W.; Li, B. W. *Appl. Phys. Lett.* **2012,** *100*, 093107.
(13) Falin, A.; Cai, Q. R.; Santos, E. J. G.; Scullion, D.; Qian, D.; Zhang, R.; Yang, Z.; Huang, S. M.; Watanabe, K.; Taniguchi, T.; Barnett, M. R.; Chen, Y.; Ruoff, R. S.; Li, L. H. *Nat. Commun.* **2017,** *8*, 15815.
(14) Li, L. H.; Chen, Y. *Adv. Funct. Mater.* **2016,** *26*, 2594-2608.
(15) Dean, C. R.; Young, A. F.; Meric, I.; Lee, C.; Wang, L.; Sorgenfrei, S.; Watanabe, K.; Taniguchi, T.; Kim, P.; Shepard, K. L.; Hone, J. *Nat. Nanotechnol.* **2010,** *5*, 722-726.
(16) Li, L. H.; Santos, E. J.; Xing, T.; Cappelluti, E.; Roldán, R.; Chen, Y.; Watanabe, K.; Taniguchi, T. *Nano Lett.* **2015,** *15*, 218-223.
(17) Li, L. H.; Cervenka, J.; Watanabe, K.; Taniguchi, T.; Chen, Y. *ACS Nano* **2014,** *8*, 1457-1462.
(18) Liu, Z.; Gong, Y. J.; Zhou, W.; Ma, L. L.; Yu, J. J.; Idrobo, J. C.; Jung, J.; MacDonald, A. H.; Vajtai, R.; Lou, J.; Ajayan, P. M. *Nat. Commun.* **2013,** *4*, 2541.
(19) Li, L. H.; Xing, T.; Chen, Y.; Jones, R. *Adv. Mater. Interfaces* **2014,** *1*, 1300132.
(20) Chen, X. L.; Wu, Y. Y.; Wu, Z. F.; Han, Y.; Xu, S. G.; Wang, L.; Ye, W. G.; Han, T. Y.; He, Y. H.; Cai, Y.; Wang, N. *Nat. Commun.* **2015,** *6*, 7315.
(21) Shen, L. T.; Zhao, Y. D.; Wang, Y.; Song, R. B.; Yao, Q.; Chen, S. S.; Chai, Y. *J. Mater. Chem. A* **2016,** *4*, 5044-5050.
(22) Mahvash, F.; Eissa, S.; Bordjiba, T.; Tavares, A. C.; Szkopek, T.; Siaj, M. *Sci. Rep.* **2017,** *7*, 42139.
(23) Cai, Q.; Mateti, S.; Yang, W.; Jones, R.; Watanabe, K.; Taniguchi, T.; Huang, S.; Chen, Y.; Li, L. H. *Angew. Chem. Int. Ed.* **2016,** *55*, 8405-8409.
(24) Cai, Q.; Mateti, S.; Watanabe, K.; Taniguchi, T.; Huang, S.; Chen, Y.; Li, L. H. *ACS Appl. Mater. Interfaces* **2016,** *8*, 15630-15636.
(25) Cai, Q. R.; Du, A. J.; Gao, G. P.; Mateti, S.; Cowie, B. C. C.; Qian, D.; Zhang, S.; Lu, Y. R.; Fu, L.; Taniguchi, T.; Huang, S. M.; Chen, Y.; Ruoff, R. S.; Li, L. H. *Adv. Funct.Mater.* **2016,** *26*, 8202-8210.

(26) Sichel, E. K.; Miller, R. E.; Abrahams, M. S.; Buiocchi, C. J. *Phys. Rev. B* **1976,** *13*, 4607-4611.
(27) Simpson, A.; Stuckes, A. D. *J. Phys. Part C Solid* **1971,** *4*, 1710-1718.
(28) Zhi, C. Y.; Bando, Y.; Tang, C. C.; Kuwahara, H.; Golberg, D. *Adv. Mater.* **2009,** *21*, 2889-2893.
(29) Wang, X. B.; Pakdel, A.; Zhang, J.; Weng, Q. H.; Zhai, T. Y.; Zhi, C. Y.; Golberg, D.; Bando, Y. *Nanoscale Res. Lett.* **2012,** *7*, 662.
(30) Wang, Z. F.; Fu, Y. Q.; Meng, W. J.; Zhi, C. Y. *Nanoscale Res. Lett.* **2014,** *9*, 643.
(31) Zhu, H. L.; Li, Y. Y.; Fang, Z. Q.; Xu, J. J.; Cao, F. Y.; Wan, J. Y.; Preston, C.; Yang, B.; Hu, L. B. *ACS Nano* **2014,** *8*, 3606-3613.
(32) Yu, J. H.; Mo, H. L.; Jiang, P. K. *Polym. Advan. Technol.* **2015,** *26*, 514-520.
(33) Huang, T.; Zeng, X. L.; Yao, Y. M.; Sun, R.; Meng, F. L.; Xu, J. B.; Wong, C. P. *RSC Adv.* **2016,** *6*, 35847-35854.
(34) Nagaoka, S.; Jodai, T.; Kameyama, Y.; Horikawa, M.; Shirosaki, T.; Ryu, N.; Takafuji, M.; Sakurai, H.; Ihara, H. *RSC Adv.* **2016,** *6*, 33036-33042.
(35) Wang, F. F.; Zeng, X. L.; Yao, Y. M.; Sun, R.; Xu, J. B.; Wong, C. P. *Sci. Rep.* **2016,** *6*, 19394.
(36) Zheng, J. C.; Zhang, L.; Kretinin, A. V.; Morozov, S. V.; Wang, Y. B.; Wang, T.; Li, X. J.; Ren, F.; Zhang, J. Y.; Lu, C. Y.; Chen, J. C.; Lu, M.; Wang, H. Q.; Geim, A. K.; Novoselov, K. S. *2D Mater.* **2016,** *3*, 011004.
(37) Bao, J.; Edwards, M.; Huang, S. R.; Zhang, Y.; Fu, Y. F.; Lu, X. Z.; Yuan, Z. C.; Jeppson, K.; Liu, J. *J. Phys. D* **2016,** *49*, 265501.
(38) Yang, W.; Berthou, S.; Lu, X. B.; Wilmart, Q.; Denis, A.; Rosticher, M.; Taniguchi, T.; Watanabe, K.; Feve, G.; Berroir, J. M.; Zhang, G. Y.; Voisin, C.; Baudin, E.; Placais, B. *Nat. Nanotechnol.* **2018,** *13*, 47-52.
(39) Sevik, C.; Kinaci, A.; Haskins, J. B.; Cagin, T. *Phys. Rev. B* **2011,** *84*, 085409.
(40) Lindsay, L.; Broido, D. A. *Phys. Rev. B* **2011,** *84*, 155421.
(41) Sevik, C.; Kinaci, A.; Haskins, J. B.; Cagin, T. *Phys. Rev. B* **2012,** *86*, 075403.
(42) Lindsay, L.; Broido, D. A. *Phys. Rev. B* **2012,** *85*, 035436.
(43) Mortazavi, B.; Pereira, L. F. C.; Jiang, J. W.; Rabczuk, T. *Sci. Rep.* **2015,** *5*, 13228.
(44) Cepellotti, A.; Fugallo, G.; Paulatto, L.; Lazzeri, M.; Mauri, F.; Marzari, N. *Nat. Commun.* **2015,** *6*, 6400.
(45) Jo, I.; Pettes, M. T.; Kim, J.; Watanabe, K.; Taniguchi, T.; Yao, Z.; Shi, L. *Nano. Lett.* **2013,** *13*, 550-554.
(46) Zhou, H. Q.; Zhu, J. X.; Liu, Z.; Yan, Z.; Fan, X. J.; Lin, J.; Wang, G.; Yan, Q. Y.; Yu, T.; Ajayan, P. M.; Tour, J. M. *Nano Res.* **2014,** *7*, 1232-1240.
(47) Alam, M. T.; Bresnehan, M. S.; Robinson, J. A.; Haque, M. A. *Appl. Phys. Lett.* **2014,** *104*, 013113.
(48) Ziyuan, L.; Chunru, L.; Yang, C. *2D Mater.* **2016,** *3*, 041009.
(49) Lee, G. H.; Cooper, R. C.; An, S. J.; Lee, S.; van der Zande, A.; Petrone, N.; Hammerherg, A. G.; Lee, C.; Crawford, B.; Oliver, W.; Kysar, J. W.; Hone, J. *Science* **2013,** *340*, 1073-1076.
(50) Wang, C. R.; Guo, J.; Dong, L.; Aiyiti, A.; Xu, X. F.; Li, B. W. *Sci. Rep.* **2016,** *6*, 25334.
(51) Castellanos-Gomez, A.; Buscema, M.; Molenaar, R.; Singh, V.; Janssen, L.; van der Zant, H. S. J.; Steele, G. A. *2D Mater.* **2014,** *1*, 011002.
(52) Taniguchi, T.; Watanabe, K. *J. Cryst. Growth* **2007,** *303*, 525-529.

(53) Li, L.; Li, L. H.; Chen, Y.; Dai, X. J.; Lamb, P. R.; Cheng, B. M.; Lin, M. Y.; Liu, X. *Angew. Chem.* **2013,** *125*, 4306-4310.
(54) Cai, Q.; Scullion, D.; Falin, A.; Watanabe, K.; Taniguchi, T.; Chen, Y.; Santos, E. J. G.; Li, L. H. *Nanoscale* **2017,** *9*, 3059-3067.
(55) Zhang, X.; Sun, D. Z.; Li, Y. L.; Lee, G. H.; Cui, X.; Chenet, D.; You, Y. M.; Heinz, T. F.; Hone, J. C. *ACS Appl. Mater. Interfaces* **2015,** *7*, 25923-25929.
(56) Yan, R. S.; Simpson, J. R.; Bertolazzi, S.; Brivio, J.; Watson, M.; Wu, X. F.; Kis, A.; Luo, T. F.; Walker, A. R. H.; Xing, H. G. *ACS Nano* **2014,** *8*, 986-993.
(57) Lu, J.; Ren, Q. J.; Sun, L. X.; Yu, J.; Chen, Y.; Shen, X. C.; Chen, Z. H. *Appl. Phys. Express* **2014,** *7*, 022401.
(58) Anees, P.; Valsakumar, M. C.; Panigrahi, B. K. *Phys. Chem. Chem. Phys.* **2016,** *18*, 2672-2681.
(59) Nair, R. R.; Blake, P.; Grigorenko, A. N.; Novoselov, K. S.; Booth, T. J.; Stauber, T.; Peres, N. M. R.; Geim, A. K. *Science* **2008,** *320*, 1308-1308.
(60) Beiranvand, R.; Valedbagi, S. *Diam. Rela.t Mater.* **2015,** *58*, 190-195.
(61) Song, L.; Ci, L. J.; Lu, H.; Sorokin, P. B.; Jin, C. H.; Ni, J.; Kvashnin, A. G.; Kvashnin, D. G.; Lou, J.; Yakobson, B. I.; Ajayan, P. M. *Nano Lett.* **2010,** *10*, 3209-3215.
(62) Stehle, Y.; Meyer, H. M.; Unocic, R. R.; Kidder, M.; Polizos, G.; Datskos, P. G.; Jackson, R.; Smirnov, S. N.; Vlassiouk, I. V. *Chem. Mater.* **2015,** *27*, 8041-8047.
(63) Lindsay, L.; Broido, D. A.; Mingo, N. *Phys. Rev. B* **2011,** *83*, 235428.
(64) Chen, Z. Y.; Darancet, P.; Wang, L.; Crowther, A. C.; Gao, Y. D.; Dean, C. R.; Taniguchi, T.; Watanabe, K.; Hone, J.; Marianetti, C. A.; Brus, L. E. *ACS Nano* **2014,** *8*, 2943-2950.
(65) Yoon, D.; Son, Y. W.; Cheong, H. *Nano Lett.* **2011,** *11*, 3227-3231.
(66) Pease, R. S. *Acta Crystallogr* **1952,** *5*, 356-361.
(67) Plimpton, S. *J. Comput. Phys.* **1995,** *117*, 1-19.
(68) Tersoff, J. *Phys. Rev. B* **1988,** *37*, 6991-7000.
(69) Jones, J. E. *P R Soc Lond a-Conta* **1924,** *106*, 463-477.
(70) Kresse, G.; Hafner, J. *Phys. Rev. B* **1993,** *48*, 13115-13118.
(71) Perdew, J. P.; Burke, K.; Ernzerhof, M. *Phys. Rev. Lett.* **1996,** *77*, 3865-3868.
(72) Tkatchenko, A.; DiStasio, R. A.; Car, R.; Scheffler, M. *Phys. Rev. Lett.* **2012,** *108*, 236402.
(73) Ambrosetti, A.; Reilly, A. M.; DiStasio, R. A.; Tkatchenko, A. *J. Chem. Phys.* **2014,** *140*, 18A508.
(74) Blochl, P. E. *Phys. Rev. B* **1994,** *50*, 17953-17979.
(75) Kresse, G.; Joubert, D. *Phys. Rev. B* **1999,** *59*, 1758-1775.
(76) Togo, A.; Tanaka, I. *Scripta. Mater.* **2015,** *108*, 1-5.